(Preprint) AAS 18-244

HIGH FIDELITY COLLISION PROBABILITIES ESTIMATED USING BRUTE FORCE MONTE CARLO SIMULATIONS

Doyle T. Hall*, Stephen J. Casali*, Lauren C. Johnson*, Brent B. Skrehart* and Luis G. Baars*

The NASA Conjunction Assessment Risk Analysis team has implemented new software to estimate the probability of collision (P_c) for Earth-orbiting satellites. The algorithm employs a "brute force Monte Carlo" (BFMC) method which differs from most other methods because it uses orbital states and covariances propagated from their orbit determination epoch times using the full set of Astrodynamics Support Workstation higher order theory models, including the High Accuracy Satellite Drag Model. This paper describes the BFMC algorithm, presents comparisons of BFMC P_c estimates to those calculated using other methods, and discusses the implications for conjunction risk assessment.

INTRODUCTION

The NASA Conjunction Assessment Risk Analysis (CARA) team estimates the probability of collision for a specific set of high value Earth-orbiting satellites. The CARA processing system first detects candidate close encounters up to ten days in advance using a screening-volume approach based on the latest available satellite tracking data and orbit determination (OD) state and covariance solutions.[1,2] For each candidate conjunction, CARA assesses the collision risk using a set of well-established semi-analytical P_c estimation methods[3,4] which are relatively computationally efficient because they employ several simplifying assumptions, including linear trajectories. Unfortunately, such methods can potentially fail to provide accurate P_c estimates for specific conjunction geometries, including long-term or repeating encounters between closely spaced objects.[4] These specific conjunctions can be addressed using Monte Carlo (MC) simulations.[5]

The CARA team has implemented software to calculate P_c estimates employing a "brute force Monte Carlo" or BFMC algorithm. The method can be computationally intensive because it uses high fidelity Special Perturbations (SP) orbital propagation[6] within an MC approach that has been described in detail previously.[7] Specifically, the most advanced mode of the BFMC software repeatedly performs the following algorithmic steps: 1) sample SP states from their probability density functions (PDFs) of the primary and secondary satellites at their respective OD epoch times; 2) use these sampled SP states to propagate high fidelity estimates of the state vectors of two satellites forward in time throughout the entire period of interest for collision risk assessment, explicitly checking if the intervening distance ever becomes less than the combined "hard-body" radii of the two satellites; and 3) if so, register that a simulated collision has occurred at the time of first contact between the two spheres defined by those radii. These steps need to be repeated until sufficient simulated collisions have been registered to provide a P_c estimate to a desired accuracy.

* Research Analyst, Omitron Inc., 555 E. Pikes Peak Ave, #205 Colorado Springs, CO 80903.

The BFMC algorithm differs from most other P_c estimation methods in two ways. First, it uses the complete SP orbital states and covariances, enabling high fidelity trajectory propagation. Second, in its most advanced mode of operation, BFMC uses only the SP states and covariances estimated at the OD epoch times, instead of relying on states and covariances predicted at the nominal time of closest approach (TCA) for the conjunction. The SP states comprise six equinoctial orbital elements, supplemented by two additional state parameters that account for the effects of orbital perturbations, including atmospheric drag and solar radiation pressure.[6,7]

Because BFMC employs SP states and equinoctial orbital elements natively, it can be used for studying P_c inaccuracies introduced by using Cartesian or other state representations.[7] BFMC also incorporates the latest version of the Jacchia-Bowman atmospheric density model[8] plus the associated Dynamic Calibration Atmosphere (DCA) for the High Accuracy Satellite Drag Model (HASDM)[9] and exactly matches the currently operational SP software configuration of the Astrodynamics Support Workstation (ASW).[10,11] Great care has been taken to ensure that all SP propagations are performed using the most recent and accurate input data, including the latest updates available for orbital states and atmospheric parameters.

This paper describes the BFMC algorithm in detail, presents comparisons of the high fidelity BFMC P_c estimates to those calculated using other methods, and discusses the implications for satellite conjunction risk assessment.

PREVIOUS WORK

Collision probabilities between tracked Earth-orbiting satellites have been discussed extensively during the past few decades, including methods that use semi-analytical approaches as well as more computationally intensive Monte Carlo approaches.

Semi-Analytical Collision Probability Methods

Many authors have formulated and discussed semi-analytical P_c methods (see references 3, 4, 12-17, and references therein). In 1992, Foster and Estes[3] introduced a method that employs three simplifying assumptions: 1) the relative satellite motion can be approximated as linear during the conjunction, 2) the uncertainties on the relative satellite positions during the conjunction can be approximated using a single, constant covariance matrix, and 3) the uncertainties on the satellite velocities can be neglected altogether. These assumptions make the mathematical problem significantly more tractable, and ultimately allow P_c values to be approximated semi-analytically using 2-dimensional (2D) numerical integration.[3,4] In 2000, Akella and Alfriend[9] also employed these assumptions, but reformulated the theory to demonstrate that the collision probability can be alternatively be expressed as an integral over time

$$P_c = \int_{\tau_a}^{\tau_b} R_c(t)\, dt \tag{1}$$

where the integrand $R_c(t)$ represents a collision probability rate (also see reference 14), which can itself be calculated using 2D numerical integration. In a linear-motion encounter, only one close approach (CA) occurs, meaning that $R_c(t)$ has a single peak in time, so the integration limits can be taken as $\tau_a = -\infty$ and $\tau_b = \infty$. Akella and Alfriend[12] show that the infinitely-bounded time integral part of the expression above can be performed analytically, ultimately yielding an expression for P_c with the same form as originally presented by Foster and Estes.[3]

Most conjunctions between tracked satellites can be approximated accurately using the "2D P_c" methods of Foster and Estes[3] and Akella and Alfriend.[12] However, some conjunctions do not sat-

isfy all three of the 2D P_c assumptions stated above, and must be addressed using a different approach.[4,5] Several authors have formulated semi-analytical approaches relaxing the 2D P_c assumptions.[4,13-17] This analysis focuses on using MC methods for this purpose.

Monte Carlo Collision Probability Methods

Collision probabilities can be estimated using MC simulations.[5,7] These can be computationally intensive because they require repeatedly performing the following steps: 1) sample the orbital state PDFs of the primary and secondary satellites; 2) use the sampled states to propagate state vectors throughout the risk assessment period, determining if the distance between the objects ever becomes less than a combined hard-body protection radius; and 3) if so, register that a simulated collision has occurred.[18] These steps need to be repeated until enough collisions have been registered to provide sufficiently accurate statistical results, which may require a large number of samples depending on the conjunction. Step 2 requires the most computation, especially for propagation schemes that use complex dynamical models.

In 2011, Sabol *et al.*[7] described an MC approach using high fidelity SP orbital propagation, which employs a complex and accurate special perturbations dynamical model.[6,10,11] That analysis describes two important aspects of the SP MC approach. First, using a Cartesian orbital state representation in the simulations should be avoided because it inaccurately models satellite state uncertainties — a drawback not suffered when using an SP state representation expressed in equinoctial orbital elements supplemented by additional state parameters.[7,19-21] Second, SP state sampling and propagation can be performed in two distinctly different ways.[7] States can be sampled from PDFs estimated at the OD epoch times for the primary and secondary satellites, and then propagated forward in time throughout a collision risk assessment period. Alternatively, states can be sampled from PDFs predicted for a conjunction's nominal TCA and propagated from that point in time. In this analysis, these two approaches will be referred to as "from-epoch" and "from-TCA," respectively.

BRUTE FORCE MONTE CARLO COLLISION PROBABILITY ALGORITHM

The BFMC algorithm presented here extends the method originally developed by Sabol *et al.*[7] so that it can be applied to actual conjunctions experienced by CARA's set of protected primary satellites. The BFMC software has two fundamental modes of operation, corresponding to the from-epoch and from-TCA sampling+propagation approaches discussed above. The from-epoch approach represents BFMC's most advanced P_c estimation mode, and is described in detail first, followed by a description of the from-TCA approach.

Special Perturbations Orbital States and Covariances

An SP orbital state is represented by an 8×1 column vector, $\mathbf{X} = [n, a_f, a_g, \chi, \psi, \lambda_M, B, S]^T$, with the first six elements denoting the satellite's equinoctial orbital elements, and the last two a ballistic coefficient plus a solar radiation pressure parameter.[6,22-24] The ASW OD process[2,6,10,11] analyzes multiple tracking observations of a satellite to estimate a mean state, $\overline{\mathbf{X}}_0$, at an OD epoch time, t_0. (This analysis uses a subscript "0" to denote quantities associated with an OD epoch, but only when required for clarity.) The epoch t_0 typically coincides with the time of the latest tracking observation incorporated into the OD analysis.

The actual state for a satellite at epoch differs from the estimated mean state because of measurement and modeling uncertainties, $\mathbf{X}_{0,\text{actual}} = \overline{\mathbf{X}}_0 + \mathbf{x}_0$, and the OD process also provides an estimate of the 8×8 covariance matrix, $\mathbf{P}_0 = \langle \mathbf{x}_0 \mathbf{x}_0^T \rangle$, based on measurement residuals.[2,6,10,23,24] The epoch state uncertainty PDF can be approximated using a "single-Gaussian" representation,[21] $\rho_0(\mathbf{X}_0; \overline{\mathbf{X}}_0, \mathbf{P}_0) = \mathcal{N}(\mathbf{X}_0 - \overline{\mathbf{X}}_0, \mathbf{P}_0)$, where $\mathcal{N}$ denotes a multi-variate normal (MVN) function

$$\mathcal{N}(\mathbf{x}, \mathbf{P}) = [\det(2\pi\mathbf{P})]^{-1/2} \left[\exp\left(-\frac{\mathbf{x}^T\mathbf{P}^{-1}\mathbf{x}}{2}\right)\right] \quad (2)$$

The epochs, mean states and covariances $(t_0, \overline{\mathbf{X}}_0, \mathbf{P}_0)$ can be derived from the *Vector Covariance Message* (VCM) produced by the ASW OD processing system.[10,11]

The SP epochs, mean states and covariances for the primary and secondary objects involved in a conjunction are denoted here as $(t_{1,0}, \overline{\mathbf{X}}_{1,0}, \mathbf{P}_{1,0})$ and $(t_{2,0}, \overline{\mathbf{X}}_{2,0}, \mathbf{P}_{2,0})$, respectively. (This analysis uses subscripts "1" and "2" to denote quantities associated with the primary and secondary, but, again, only when required for clarity.) Typically, the two OD epochs do not coincide, $t_{1,0} \neq t_{2,0}$, and both typically precede the nominal conjunction TCA by 0.5 to 10 days in CARA processing. Because VCMs for both the primary and secondary object are used as inputs for from-epoch processing, BFMC's from-epoch mode is also referred to as "VCM mode."

Special Perturbations Propagation

SP states can be propagated to predict high fidelity future Earth-Centered Inertial (ECI) reference frame satellite position vectors,[6] denoted symbolically here as $\mathbf{r}(t; t_0, \mathbf{X}_0, \boldsymbol{\mathcal{D}})$, where $\boldsymbol{\mathcal{D}}$ represents an ensemble of model and environmental data sets required for SP propagation. (The contents of $\boldsymbol{\mathcal{D}}$ are described in more detail later.) Similarly, SP mean states and covariances can be propagated[6,22-24] and denoted symbolically as $\overline{\mathbf{X}}(t; t_0, \overline{\mathbf{X}}_0, \boldsymbol{\mathcal{D}})$ and $\mathbf{P}(t; t_0, \overline{\mathbf{X}}_0, \mathbf{P}_0, \boldsymbol{\mathcal{D}})$, respectively. Note, in this analysis some or all of the function arguments listed to the right of semicolons may be suppressed for brevity. For example, a position vector might be expressed in one of the following three ways: $\mathbf{r}(t) = \mathbf{r}(t; t_0, \mathbf{X}_0) = \mathbf{r}(t; t_0, \mathbf{X}_0, \boldsymbol{\mathcal{D}})$.

Sampled Orbital States

Samples can be drawn from an MVN PDF by applying Eigen-decomposition to the covariance matrix[25]

$$\mathbf{P} = \mathbf{V}\boldsymbol{\Lambda}\mathbf{V}^T \quad (3)$$

where $\mathbf{V}$ is a unitary matrix containing orthogonal eigenvector columns, $\mathbf{V}_i$, and $\boldsymbol{\Lambda}$ is a diagonal matrix of associated eigenvalues, Λ_i. The k^{th} sampled state, $\mathbf{Y}^k$, can be generated using

$$\mathbf{Y}^k = \overline{\mathbf{X}} + \sum_i \left[\varrho_i^k \mathbf{V}_i \sqrt{\Lambda_i}\right] \quad (4)$$

where $\{\varrho_i^k\}$ represents a set of independent normal deviates[26] (such as those returned by Matlab's *randn* function). This sampling method fails for non-positive definite (NPD) covariances, for which $\min(\Lambda_i) < 0$, because it produces states with non-zero imaginary components. Previous analysis indicates[25] that such NPD covariances have a variety of causes, and typically possess just one negative eigenvalue that is only slightly negative relative to the largest eigenvalue. NPD SP state epoch covariances, $\mathbf{P}_0$, occur very rarely in CARA processing; NPD propagated covariances, $\mathbf{P}(t; t_0, \overline{\mathbf{X}}_0, \mathbf{P}_0)$, occur somewhat more often, especially for long propagation intervals $t - t_0$. BFMC avoids NPD-induced sampling failures by replacing Λ_i in eq. (4) with $\max(0, \Lambda_i)$.[25]

Simulated Collisions

BFMC's from-epoch, VCM mode simulates collisions by using sampled primary and secondary SP states to propagate state vectors forward in time from their OD epochs, explicitly checking if the intervening distance between the two objects ever becomes less than a threshold miss distance, H. (Ideally, H represents the combined hard-body radii of the two objects, if both are known, but also can represent an imposed hard-body protection distance.) BFMC repeats this process for a large number of sampling trials, $k = 1 \ldots N_s$. For each trial, BFMC generates independently sampled SP states for the primary and secondary objects, $\mathbf{Y}_{1,0}^k$ and $\mathbf{Y}_{2,0}^k$, respectively. BFMC does not

reuse any state samples or propagations during the simulation; such reuse can increase the efficiency of the MC calculations but can lead to underestimated confidence intervals.[27] The time-dependent intervening distance between the two objects for the k^{th} trial can be written

$$r_{2,1}^{k}(t) = \left|\mathbf{r}_2\left(t; t_{2,0}, \mathbf{Y}_{2,0}^{k}\right) - \mathbf{r}_1\left(t; t_{1,0}, \mathbf{Y}_{1,0}^{k}\right)\right| \tag{5}$$

For a risk assessment interval $\tau_a < t \leq \tau_b$, the CA distance and time for the k^{th} trial can be found numerically as follows:

$$r_{ca}^{k} = \min_{\tau_a < t \leq \tau_b}[r_{2,1}^{k}(t)] \qquad \text{and} \qquad t_{ca}^{k} = \arg\min_{\tau_a < t \leq \tau_b}[r_{2,1}^{k}(t)] \tag{6}$$

If $r_{ca}^{k} \geq H$, then no collision could have occurred during the interval. However, if $r_{ca}^{k} < H$ and $r_{2,1}^{k}(\tau_a) \geq H$, then a collision must have occurred. In general, BFMC registers a simulated collision for the k^{th} trial if and only if there exists a "time of first contact" or t_{fc}, which is carefully defined here as the earliest time that simultaneously satisfies the following three conditions:

$$r_{2,1}^{k}\left(t_{fc}\right) = H \qquad \text{and} \qquad \dot{r}_{2,1}^{k}\left(t_{fc}\right) < 0 \qquad \text{and} \qquad \tau_a < t_{fc} \leq \tau_b \tag{7}$$

The first condition requires the two hard-body spheres to be in contact, the second that the objects be approaching one another, and the third that the contact occurs during the specified risk assessment interval. Trials that do not possess such a first contact time represent "misses" in which no collision occurs during the risk assessment interval. Each trial that does have a first contact time constitutes a simulated collision or "hit", which is registered as occurring at the time of first contact. The summed number of hits for all trials can easily be calculated and denoted $N_c(\tau_a, \tau_b)$, or just N_c for brevity.

BFMC From-Epoch or VCM Mode Collision Probabilities

Dividing the number of hits by the number of sampling trials yields the best-estimate collision probability from the MC simulation

$$\tilde{P}_c = \tilde{P}_c(\tau_a, \tau_b) = N_c(\tau_a, \tau_b)/N_s \tag{8}$$

For $N_c \gg 1$, the 95% confidence interval can usually be approximated as $\tilde{P}_c \pm [1.96\sqrt{N_c}/N_s]$, but a more accurate, asymmetric confidence interval can be estimated for all $N_c \geq 0$ using the Clopper-Pearson method[28,29] (e.g., Matlab's *binofit* function) or other methods.[30]

Because of the careful definition of the first contact time, t_{fc}, this collision probability algorithm can be applied to arbitrarily short or long time intervals, $\tau_a < t \leq \tau_b$, and will always yield a number of hits in the range $0 \leq N_c \leq N_s$, and a best-estimate probability in the range $0 \leq \tilde{P}_c \leq 1$. For temporally-isolated conjunctions, BFMC should be applied to a time interval that closely brackets the single peak in probability rate, but remains sufficiently wide to obtain an accurate total probability estimate.[18,31] However, for closely-spaced orbiting objects, which can have long-duration and/or repeating conjunctions,[17,18,32] the interval can be extended to span an arbitrarily large number of probability rate peaks. This means that BFMC's VCM mode is general enough to perform self-consistent, multi-day risk assessments even for this difficult class of satellite interaction. The CARA team continues to analyze how to use BFMC optimally to estimate probabilities for such extended, multi-encounter interactions. This analysis, however, restricts application of BFMC to temporally-isolated conjunctions for which a time interval $\tau_a < t \leq \tau_b$ can be defined that closely brackets a single peak in probability rate (as shown in the bottom panels of Figures 1 and 4).

BFMC From-Epoch or VCM Mode Collision Probability Rates

Because the algorithm presented above can be used for time intervals of arbitrary duration, it can also be applied to a sequence of very short time intervals, or bins, that jointly span the entire risk assessment period. This allows MC collision probability rates to be estimated as follows. Equally spaced time bin mid-points can be defined as $T_j = \tau_a + (j - 1/2)\Delta T$, where $j = 1 \ldots N_{bin}$ and $\Delta T = 2\,\delta T = (\tau_b - \tau_a)/N_{bin}$. The number of hits in the j^{th} bin can be easily computed and denoted $N_c\big(T_j - \delta T, T_j + \delta T\big)$, allowing the collision rate at any time during the risk assessment interval $\tau_a < t \leq \tau_b$ to be estimated by averaging over each bin:

$$\tilde{R}_c(t) = (N_s\,\Delta T)^{-1}\big[N_c\big(T_j - \delta T, T_j + \delta T\big)\big] \qquad \text{for} \qquad T_j - \delta T < t \leq T_j + \delta T \tag{9}$$

It is straightforward to show that integrating $\tilde{R}_c(t)$ from τ_a to τ_b yields $\tilde{P}_c$.

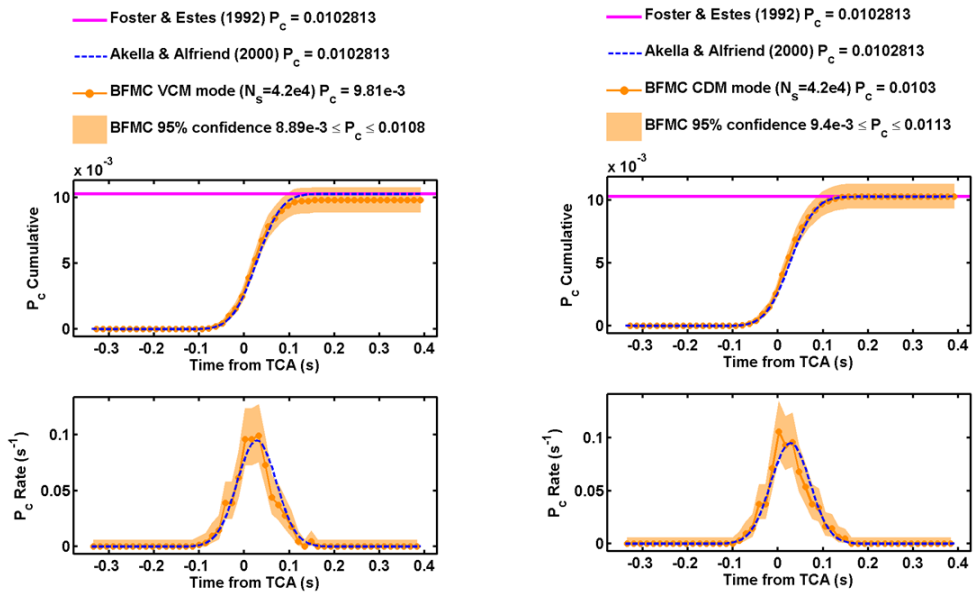

Figure 1. Estimated cumulative P_c (top panels) and P_c rate (bottom panels) from BFMC's VCM mode (left panels) and CDM mode (right panels), for a conjunction between NASA's Aqua satellite and a debris object.

Figure 1 shows plots of BFMC collision probabilities and probability rates estimated using equations (8) and (9), respectively, for a conjunction between NASA's Aqua satellite and a debris object. Specifically, the top left panel shows VCM mode $\tilde{P}_c(\tau_a, t)$ estimates, and the bottom left panel shows VCM mode $\tilde{R}_c(t)$ estimates. Orange dots show estimates for each bin and the light orange shaded region represents the associated 95% confidence uncertainty intervals.[28,29] Figure 1 also shows 2D P_c estimates[3,12] which agree well with the BFMC estimates, as is the case with the vast majority of the temporally-isolated conjunctions analyzed here (as discussed in more detail later).

BFMC From-TCA or CDM Mode Collision Probabilities and Rates

The discussion above focuses on the from-epoch sampling+propagation approach used by BFMC's VCM mode. This section explains BFMC's other principal mode, which uses a from-TCA approach that is significantly less computationally intensive. Because all input data required for from-

TCA processing can be derived from a *Conjunction Data Message* (CDM),[18,25,32] this is also called "CDM mode."

BFMC's VCM mode samples 8×1 SP state vectors from estimated OD-epoch PDFs and uses those states to calculate position vectors with high-fidelity SP propagation. BFMC's CDM mode differs in two fundamental ways. First, it samples 6×1 equinoctial element state vectors from marginalized PDFs predicted at the conjunction's nominal TCA. Second, it propagates orbital states using computationally efficient Keplerian 2-body equations of motion. As explained earlier, an SP mean state predicted at TCA can be denoted $\overline{\mathbf{X}}(t = \text{TCA}; t_0, \overline{\mathbf{X}}_0, \boldsymbol{\mathcal{D}})$. The first six elements of this 8×1 vector represent the best-estimate prediction for the mean equinoctial state, denoted here as the 6×1 vector $\overline{\mathbf{X}}'$. (In this analysis, primes denote TCA, equinoctial state quantities). Similarly, the 8×8 SP covariance matrix predicted at TCA can be denoted $\mathbf{P}(t = \text{TCA}; t_0, \overline{\mathbf{X}}_0, \mathbf{P}_0, \boldsymbol{\mathcal{D}})$. The upper-left 6×6 part of this matrix represents the marginalized equinoctial state covariance, denoted here as $\mathbf{P}'$.

TCA equinoctial element states and covariances for the primary and secondary objects, $(\overline{\mathbf{X}}_1', \mathbf{P}_1')$ and $(\overline{\mathbf{X}}_2', \mathbf{P}_2')$, respectively, can be derived from a CDM. Predicted position vectors propagated from these TCA equinoctial states using 2-body equations of motion[6,22,23] are denoted here as $\mathbf{r}_1'(t)$ and $\mathbf{r}_2'(t)$, respectively. At this point, the algorithm for BFMC's CDM mode can be formulated in the same way as described in the previous sections, but with these CDM mode quantities substituted for their original VCM mode counterparts. Specifically, the nominal TCA for the conjunction should be substituted for both epoch times $t_{1,0}$ and $t_{2,0}$; the position vector $\mathbf{r}_1'(t)$ should be substituted for $\mathbf{r}_1(t)$; $\overline{\mathbf{X}}_1'$ for $\overline{\mathbf{X}}_{1,0}$; $\mathbf{P}_1'$ for $\mathbf{P}_{1,0}$; etc.

Because the CDM mode employs 2-body propagation, it must be restricted to relatively short risk assessment intervals $\tau_a < t \leq \tau_b$ near the conjunction's nominal TCA, because it neglects orbital perturbations that can affect the orbital motion over longer time scales. For this reason, CDM mode can only be applied to temporally-isolated conjunctions with durations[4,31] that are very short relative to the minimum orbital period of the two objects.[18] This restriction does not apply to BFMC's VCM mode, because it employs only high fidelity SP propagation. CDM mode risk assessment time intervals could conceivably be extended if a higher-fidelity propagator were used, as would be required for extended or repeating events. However, any situations in which the CDM mode 2-body approach would be inadequate can already be addressed by BFMC's VCM mode.

The right panels of Figure 1 show $\tilde{P}_c(\tau_a, t)$ and $\tilde{R}_c(t)$ estimates produced by BFMC's CDM mode. Figure 1 demonstrates that the VCM and CDM modes produce statistically equivalent results for this conjunction. This CDM vs VCM mode equivalence has been found to hold for all temporally-isolated conjunctions analyzed so far, as discussed in detail later. Figure 1 also demonstrates that, for this Aqua satellite conjunction, both BFMC estimates agree well with the 2D P_c approximation: VCM-$P_c \approx$ CDM-$P_c \approx$ 2D-$P_c \approx 10^{-2}$. This BFMC vs 2D P_c equivalence has been found to hold for the vast majority of temporally-isolated conjunctions analyzed here, but a small fraction show statistically significant differences, also discussed in detail later.

BRUTE FORCE MONTE CARLO SOFTWARE IMPLEMENTATION

The main BFMC software module encodes the sampling, propagation, and collision simulation algorithms described above, implemented in compiled FORTRAN that links with ASW software libraries.[10] In addition, a set of pre-processing modules collect and assemble the input data required for BFMC operation, and a set of post-processing modules produce analysis summaries and plots. The pre- and post-processing modules consist predominantly of Matlab codes.

Input Data Required for CDM Mode

The input data required for BFMC's CDM mode can be derived from the CDMs themselves. For archived conjunctions, pre-existing CDMs originally created by the ASW system can be retrieved from CARA's database. For a current conjunction, with a TCA predicted in the near future, a new CDM can be created using the quantities $(t_{1,0}, \overline{\mathbf{X}}_{1,0}, \mathbf{P}_{1,0}, t_{2,0}, \overline{\mathbf{X}}_{2,0}, \mathbf{P}_{2,0}, \boldsymbol{\mathcal{D}})$.

Input Data Required for VCM Mode

BFMC's VCM mode requires a much larger set of inputs than CDM mode. First, it requires VCMs for both the primary and secondary objects. In addition, it requires a large ensemble of model and environmental data sets, represented collectively using the symbol $\boldsymbol{\mathcal{D}}$, to enable the high fidelity SP propagations for both the primary and secondary objects. $\boldsymbol{\mathcal{D}}$ includes up to a 70×70 array of coefficients describing Earth's gravitational field,[6] a large set of time-dependent HASDM atmospheric density model[8,9] parameters, lunar and solar gravitation parameters, solar radiation parameters, etc.[6] Some of these data sets reside in text files assembled during BFMC pre-processing, and then provided as input to the main BFMC module. Specifically, in addition to the primary+secondary VCMs themselves, BFMC's VCM mode requires the following input text files:

1. A file containing an archive of time constants, leap seconds, UT1-UTC, Δ(UT1-UTC), and polar motion data, listed at 10 day spacing.
2. A file containing solar extreme ultraviolet heating parameters required for the SP Jacchia-Bowman atmospheric density modeling.[8]
3. A file containing atmospheric density model DCA correction data with 3 hour spacing.[9]
4. A file containing a compilation of dynamic consider parameters required for SP processing, listed by satellite number, as well as HASDM compatible ballistic coefficients. (The dynamic consider parameter is used to model ASW drag parameter uncertainties related to satellite frontal area variations, solar activity, and perigee height.)

The CARA team captures data to populate these four files at regular intervals from the ASW data processing system, in order to assemble a nearly complete chronological history.

Notably, to compare BFMC CDM mode and VCM mode calculations in order to check for consistency, the same exact input data sets $\boldsymbol{\mathcal{D}}$ must be used as input for both. This means that the data $\boldsymbol{\mathcal{D}}$ used to create a pre-existing CDM, must be successfully retrieved from the database and incorporated into the four files data described above. Unfortunately, CARA's database for these four files is not comprehensive, because the periodic updates it employs do not include all of the transient updates that occur within the ASW system. In order to verify that the correct data $\boldsymbol{\mathcal{D}}$ have been gathered for archive conjunction analysis, the main BFMC module calculates the nominal conjunction TCA plus the associated states and covariances for both the primary and secondary objects. These must reproduce the associated quantities derived from the original, pre-existing CDM to within predetermined numerical tolerances in order to verify that the proper data sets $\boldsymbol{\mathcal{D}}$ have indeed been assembled. This "check-out" procedure must be passed in order to compare BFMC CDM mode and VCM mode P_c values legitimately.

It is worthwhile to note that this check-out procedure need only be performed explicitly for pre-existing CDMs, such as those retrieved from CARA's archive. It would not need to be done for a current conjunction with a TCA predicted in the near future (as encountered in operational processing, for instance) because the best data $\boldsymbol{\mathcal{D}}$ required for both CDM creation and VCM mode execution would naturally be available to the processing system at the time of execution.

Accounting for Cross Correlated Orbital State Estimates

The BFMC algorithm presented above assumes that the OD-epoch state uncertainty PDF covariances for the primary and secondary objects ($\mathbf{P}_{1,0}, \mathbf{P}_{2,0}$) are statistically independent. However, because of the way OD processing is performed,[2,6] estimated orbital state covariances can be correlated due to the use of common force-model parameters, common tracking system biases, etc.[33] Such correlations can affect P_c estimates.[33,34] The BFMC processing system naturally lends itself to correcting for cross correlation effects caused by common force-model parameters — in particular, those within the global atmospheric density model used for both state estimation and state prediction.[8] A companion BFMC paper presented at this conference by Casali *et al.*[34] formulates a method that uses the atmospheric data collected and assembled within $\boldsymbol{\mathcal{D}}$ to account for such cross correlations in the state prediction portion of the process. For most conjunctions, accounting for such prediction-phase cross correlation effects has a relatively small effect on P_c estimates. However, for conjunctions involving satellites experiencing appreciable atmospheric drag, P_c values can be increased or decreased significantly.[34] The current analysis assumes for simplicity that the covariances ($\mathbf{P}_{1,0}, \mathbf{P}_{2,0}$) have negligible cross correlation, focusing on the comparison of different MC P_c estimation methods rather than eradicating cross correlation effects in the calculation.

Measurements of Computation Speeds

Because BFMC's CDM mode employs efficient 2-body propagation, it computes more quickly than the VCM mode, which employs high fidelity SP propagation. Performance measurements using a 24 CPU core Linux workstation indicate that BFMC's main module in CDM mode can calculate at a rate of about $\mathcal{R}_{\mathrm{CDM}} \approx 10^5$ sampling trials per second using a single core. VCM mode single-core computation rates depend inversely on the summed propagation times for the primary and secondary as follows

$$\mathcal{R}_{\mathrm{VCM}} \approx \left(10 \frac{\text{trials PROPday}}{\text{CPUsec}}\right)\left[(\mathrm{TCA} - t_{1,0}) + (\mathrm{TCA} - t_{2,0})\right]^{-1} \tag{10}$$

So for an isolated conjunction in which both OD epochs precede the nominal TCA by twelve hours, i.e., $(\mathrm{TCA} - t_{1,0}) + (\mathrm{TCA} - t_{2,0}) = 1$ PROPday, about 10 VCM mode trials can be calculated per second using a single core. Using 20 cores in parallel increases this to about 200 trials per second.

Table 1. Approximate BFMC execution times for a workstation using 20 CPU cores, estimating P_c values to an accuracy of about 20% with 95% confidence.

	$P_c = 10^{-4}$	$P_c = 10^{-5}$	$P_c = 10^{-6}$	$P_c = 10^{-7}$
CDM Mode	**0.5 seconds**	**5 seconds**	**50 seconds**	**8.3 minutes**
VCM (1 PROPday)	**1.4 hours**	**14 hours**	**5.8 days**	**58 days**
VCM (10 PROPdays)	**14 hours**	**5.8 days**	**58 days**	**580 days**

Estimating P_c values to an accuracy of about 20% with 95% confidence usually requires $N_c \approx 100$ hits (which also yields a 1σ accuracy of about 10%). For a conjunction with $P_c = 10^{-4}$, this requires $N_s \approx 10^6$ sampling trials, which can be computed using CDM mode with 20 cores in about 0.5 seconds. Table 1 lists such "20-core, 100-hit" BFMC execution times for $10^{-4} \le P_c \le 10^{-7}$. The majority of important CARA conjunctions have total propagation times less than 10 days.

The measurements indicate that BFMC's CDM mode executes sampling trials about 10^4–10^5 times faster than the VCM mode, depending on the conjunction. This relative CDM/VCM speed ratio

likely applies to other computer hardware systems as well, in addition to the specific multi-core Linux workstation used for this study.

Cloud Based Implementation

Table 1 indicates that CDM mode computations using 20 workstation CPU cores in parallel can easily execute quickly enough to allow risk assessments to be performed, as well as to allow associated remediation maneuvers/activities to be planned and performed. However, VCM mode computations might require too much execution time to allow such risk assessments, especially for the smaller P_c values in Table 1. This could be addressed by employing a larger number of CPUs executing in parallel, perhaps by using a commercial or government cloud computing system. Such cloud systems offer significantly more processors (referred to here as "nodes") than can be obtained using a typical workstation, but can also have significant monetary usage costs.

To investigate this, the CARA team has implemented a cloud-based version of BFMC. Measured single-node cloud execution rates for BFMC's main module are similar to the single-core rates reported above for the Linux workstation. This means that a 2000 node cloud system could decrease the BFMC run times listed in Table 1 by roughly a factor of ~100. However, even this may not be fast enough. For instance, for a conjunction predicted five days in advance with $(\mathrm{TCA} - t_{1,0}) = (\mathrm{TCA} - t_{2,0}) = 5$ PROPdays, a 2000 node VCM mode calculation seeking a 20% accuracy estimate for $P_c = 10^{-7}$ would require ~5.8 days, which would not be complete before the TCA (and would also be extremely expensive). On the other hand, 2000 nodes could execute a $P_c = 10^{-6}$ estimate in ~14 hours, likely fast enough for risk analysis, but still very expensive.

Although cloud computing could significantly speed processing, using BFMC's advanced VCM mode systematically to estimate P_c values smaller than about 10^{-5} becomes decreasingly feasible due to both scheduling and cost constraints. However, BFMC's VCM mode can provide valuable truth data in order to determine the limitations of other less computationally intensive P_c estimation methods, including BFMC's CDM mode and the 2D P_c approximation.

ANALYSIS OF ARCHIVED CONJUNCTIONS

This section presents an analysis of a large number of historical conjunctions archived in CARA's database, first comparing CDM mode vs VCM mode P_c estimates, and subsequently comparing CDM mode P_c estimates to 2D P_c approximations.[3,12] As mentioned previously, this discussion analysis restricts these comparisons to temporally-isolated conjunctions for which the risk assessment time interval $\tau_a < t \leq \tau_b$ closely brackets a single peak in probability rate.

Comparisons of CDM Mode and VCM Mode P_c Estimates

Figure 2 shows a comparison of P_c estimates calculated using BFMC's CDM and VCM modes, for 373 high P_c conjunctions processed by the CARA system between 2017-05-01 and 2018-03-18. The top panel shows a logarithmic plot of CDM mode P_c estimates (horizontal axis) vs VCM mode P_c estimates (vertical axis); the bottom panel shows the logarithm of the VCM/CDM mode P_c ratio. Error bars show the asymmetric 95% confidence intervals estimated using the Clopper-Pearson method.[28,29] During this 10.5 month period, CARA processed a total of ~430,000 conjunctions, including 500 with 2D-$P_c > 1.5\times10^{-3}$. Among those 500, however, only the subset of 373 plotted in Figure 2 had retrievable VCM mode input data sets $\boldsymbol{\mathcal{D}}$ that passed the "check-out" procedure described previously.

A binomial proportion test can be used to test the hypothesis that BFMC's CDM mode and VCM mode produce the same P_c estimates, i.e., to test the null hypothesis that two binomial proportions are equal.[35] Applying this test to each of the 373 cases plotted in Figure 2 indicates that none

violates the null hypothesis with p-value ≤ 10^{-3}. In other words, there are no points that deviate from the 45° dashed line in the upper panel of Figure 2 at this high level of statistical confidence. Additional testing of selected conjunctions using much larger numbers of sampling trials (e.g. Figure 4) also indicates that the CDM and VCM modes produce statistically equivalent P_c estimates.

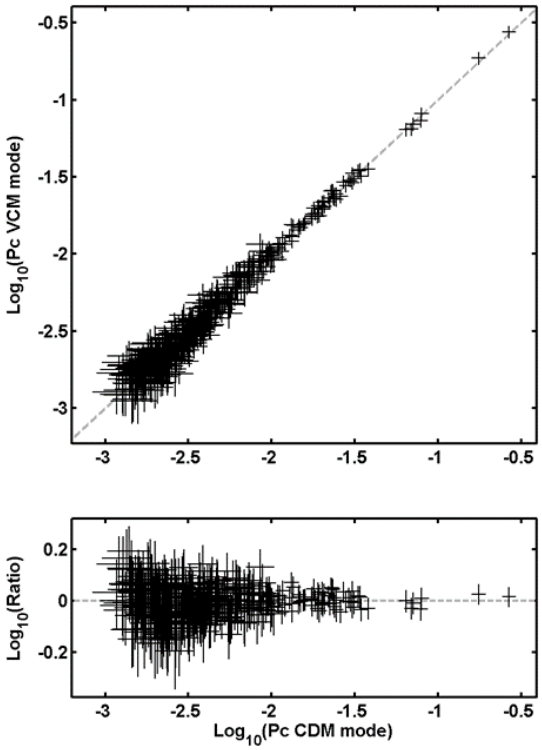

Figure 2. Comparison of BFMC CDM and VCM mode P_c estimates for 373 conjunctions.

In summary, no compellingly large deviations have been detected between BFMC's CDM mode and VCM mode P_c estimates in all of the comparison testing performed so far for temporally-isolated conjunctions, which comprise the vast majority processed by the CARA system. This close alignment occurs because BFMC's CDM mode samples equinoctial element orbital states, which resist non-Gaussian behavior due to implicit curvilinear construction.[7,19,21] On the other hand, from-TCA approaches that sample Cartesian states[18] instead of equinoctial element states can produce erroneous P_c values that differ appreciably from BFMC VCM mode estimates.

Comparisons of CDM Mode P_c Estimates and 2D P_c Approximations

Figure 3 compares P_c estimates calculated using BFMC's CDM mode to 2D P_c approximations, for 28,652 CARA conjunctions that occurred between 2017-05-01 and 2018-03-18. These conjunctions were selected using a single criterion, 2D-$P_c > 10^{-7}$, and represent events that span a large range of propagation times. The top panel shows a logarithmic plot of 2D P_c (horizontal axis) vs CDM mode P_c estimates (vertical axis). The bottom panel shows the logarithm of the P_c ratio. Conjunctions shown in black do not violate the null hypothesis test[35] that the two P_c estimates are equal at the p-value ≤ 10^{-3} significance level. However, those highlighted in yellow do violate the hypothesis at this significance level, and those in red at the higher level of p-value ≤ 10^{-6}. Overall, Figure 3 contains 99 yellow and 52 red points, which are both much greater than the numbers expected from purely statistical variations, even though they represent a very small fraction of the original 28,652 conjunctions. This provides evidence that BFMC's CDM mode yields different

results than the 2D P_c approximation, at least for a small fraction of the temporally-isolated conjunctions analyzed in this study. Major deviations occur in both directions, CDM-P_c << 2D-P_c and CDM-P_c >> 2D-P_c, with the latter type causing more concern because, for these conjunctions, the widely-employed 2D P_c approximation significantly underestimates the actual risk as indicated by the BFMC simulation. (Note, two of the conjunctions in Figure 3 with CDM-P_c << 2D-P_c corresponded to zero hits registered in the BFMC simulations, represented using downward pointing triangles with a single-sided error bar directed upward.)

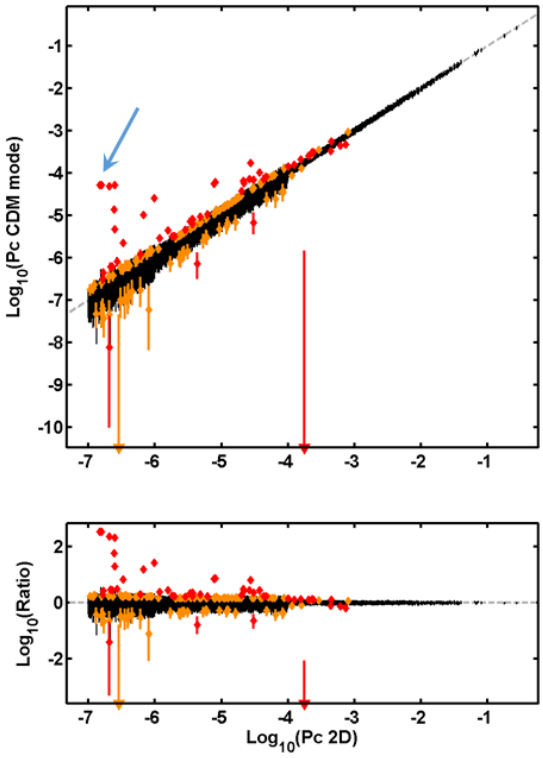

Figure 3. Comparison of BFMC CDM mode and 2D P_c estimates for 28,652 conjunctions. The blue arrow highlights the Van Allen satellite conjunction shown in Figures 4 and 5.

Many of the conjunctions with CDM-P_c >> 2D-P_c in Figure 3 have one or more of the following three characteristics: 1) involve object(s) with highly eccentric orbits, 2) have a long epoch-to-TCA propagation time of 10 days or more, and 3) have a relatively long interval between the nominal TCA and the time of peak probability rate. Many also correspond to two specific CARA supported missions, the Van Allen A and B satellites, both of which have highly eccentric orbits. The blue arrow in Figure 3 highlights a Van Allen conjunction possessing all three of these characteristics, including extended propagation times of $\mathrm{TCA} - t_{1,0} \approx 11$ PROPday for the primary Van Allen satellite, and $\mathrm{TCA} - t_{2,0} \approx 20$ PROPday for the secondary debris object, as well as a relatively long delay of about 4.5 seconds between TCA and peak probability rate. Figure 4 plots the cumulative P_c and P_c rate for this conjunction estimated using both VCM and CDM modes, with $N_s = 10^7$ sampling trials. The BFMC estimates are statistically equivalent, VCM-P_c ≈ CDM-P_c ≈ 5×10^{-5}, but both exceed the 2D-P_c ≈ 1.6×10^{-7} approximation by a factor of about 300.

The CARA analysis team continues to investigate the specific causes and circumstances of the infrequent but large BFMC-P_c vs 2D-P_c differences like those shown in Figures 3 and 4. Again,

many coincide with conjunctions involving highly eccentric orbits, extended propagation times, or long separations between TCA and peak probability rate.

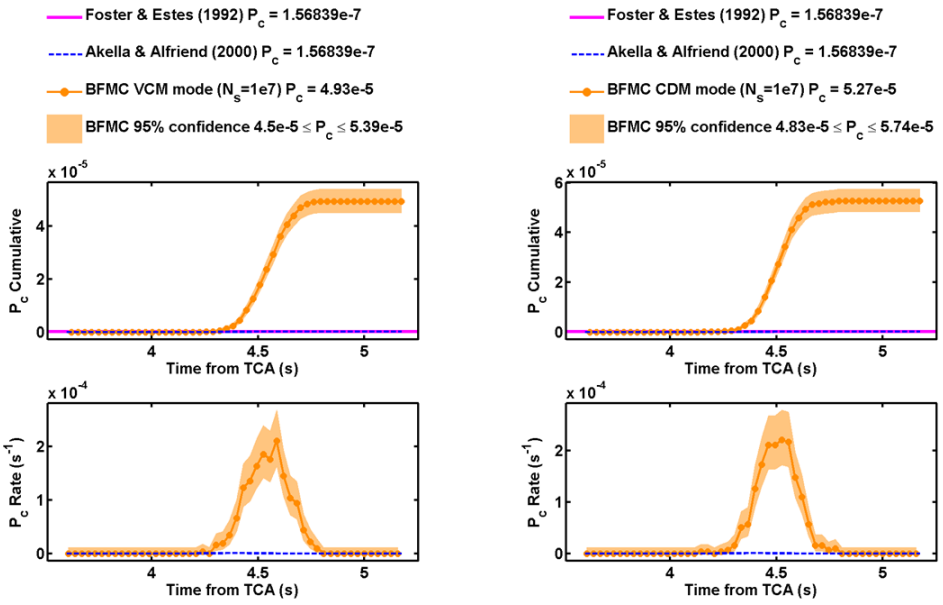

Figure 4. Estimated cumulative P_c (top panels) and P_c rate (bottom panels) from BFMC's VCM mode (left panels) and CDM mode (right panels), for a conjunction between one of NASA's Van Allen satellites and a debris object.

Comparisons of BFMC and 2D P_c Close Approach Distributions

Some insight into the infrequent conjunctions observed to have large BFMC-P_c vs 2D-P_c differences can be gained by examining the distribution of close approach events that occur in the MC simulations. Figure 5 illustrates CA distributions for the same Van Allen conjunction shown in Figure 4, produced by MC simulations using $N_s = 2.1 \times 10^6$ samples. Each dot in Figure 5 represents a CA position that occurs during one MC sampling trial. Specifically, for the k^{th} trial, the relative CA position can be plotted on a "conjunction b-plane" which is perpendicular to the relative CA velocity, as explained in more detail in Appendix A. (This conjunction b-plane is very similar to the "b-plane" used to plan and analyze planetary spacecraft encounters.[36]) Dots in Figure 5 show b-plane coordinates for each trial $\left(X_{ca}^k, Y_{ca}^k\right)$, which are related to the CA distance r_{ca}^k as follows

$$(r_{ca}^k)^2 = \left(X_{ca}^k\right)^2 + \left(Y_{ca}^k\right)^2 \tag{11}$$

So a dot for an MC trial with zero CA miss distance, $r_{ca}^k = 0$, would be located at the origin of a conjunction b-plane plot (and would also represent a hit). The two right panels on Figure 5 illustrate the CA distribution for a BFMC VCM mode simulation of the Van Allen conjunction (which look similar to those produced by the CDM mode). The left panels illustrate the CA distribution for a "2D P_c MC" simulation which employs the 2D P_c assumptions by using linear trajectories and performing TCA Cartesian state sampling neglecting velocity uncertainties.[18] The top panels show the CA distribution for all MC trials, which extend over b-plane distances of several hundred km for this conjunction. The bottom panels zoom-in to expand the view so that the Van Allen hard-body protection radius of $H = 53$ m (plotted as the green circle) can be seen more easily. Blue dots show misses (i.e., trials with $r_{ca}^k \geq H$) and red dots show hits ($r_{ca}^k < H$). Curvature in the extended BFMC CA distribution can be seen clearly in the upper right panel, but is notably absent in the 2D

P_c distribution in the upper left. The curvature in the BFMC distribution is also accompanied by many more hits (i.e., red dots in the lower right panel) than in the 2D P_c distribution (lower left).

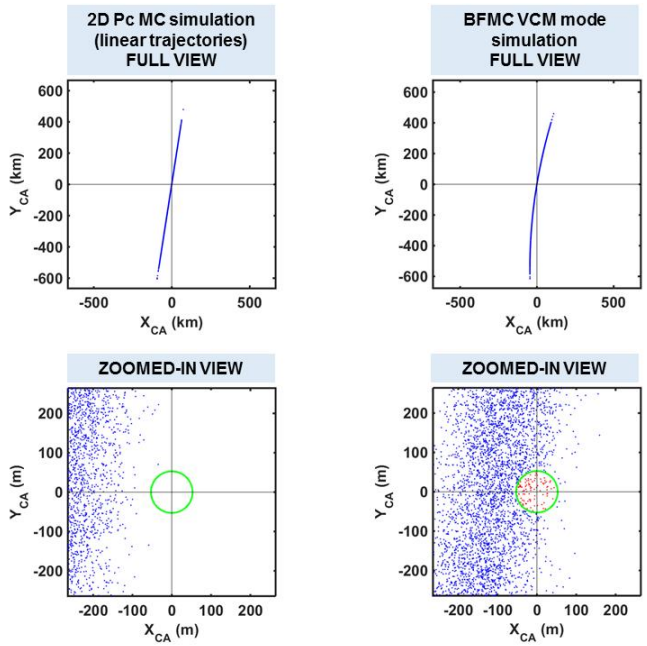

Figure 5. B-plane CA distributions for the Van Allen satellite conjunction shown in Figure 4. Curvature in the BFMC CA distribution can be seen in the upper right panel, but is absent in the 2D P_c MC distribution in the upper left.

Evidently, the 2D P_c CA distribution in the upper left panel Figure 5 lacks curvature because of the linearized-trajectory and other 2D P_c approximations, which are not invoked in the BFMC simulation. For this conjunction, the BFMC CA distribution appears to "curve toward" the hard-body region, leading to a larger number of hits and ultimately BFMC-P_c >> 2D-P_c. For other conjunctions with BFMC-P_c << 2D-P_c, similar plots show that the BFMC CA distribution appears to "curve away" from the hard-body protection region.

CONCLUSIONS

CARA's analysis using the Brute Force Monte Carlo simulation method to estimate collision probabilities for satellite conjunctions provides the following conclusions:

1. BFMC's from-epoch, VCM mode represents the most advanced and general method of estimating conjunction P_c values available to the CARA team, because it employs full eight dimensional SP states (six equinoctial elements supplemented with ballistic and solar radiation parameters) sampled at OD epoch times, estimates drag with the dynamically-calibrated HASDM atmospheric model, and performs high fidelity propagation for all sampling trials. It also provides a method to model and correct for state cross correlation effects. Because of this, BFMC's VCM mode provides valuable truth data to use when studying other P_c estimation and approximation methods.
2. The VCM mode algorithm can be applied to all risk assessment time scales, so that collision probabilities as well as probability rates can be estimated for single, temporally-isolated con-

junctions (as has been done in this analysis), or for the much more difficult class of long-duration, temporally-repeating conjunctions that can occur between closely-spaced orbiting objects (now being investigated by the CARA team).

3. VCM mode execution rates depend inversely on the summed propagation times for the primary and secondary. For a summed propagation time of 1 day, a single modern CPU can compute about 10 VCM mode sampling trials per second.
4. Slow execution rates prevent BFMC's VCM mode from being used systematically to estimate P_c values smaller than about 10^{-5} for conjunction risk assessment, even when using large (and expensive) cloud-based computing systems.
5. BFMC's from-TCA, CDM mode computes sampling trials approximately 10^4 to 10^5 times faster than the VCM mode, depending on the conjunction. This is achieved by employing six dimensional equinoctial element states sampled at the conjunction's nominal TCA, and utilizing relatively efficient Keplerian 2-body propagation.
6. BFMC's CDM mode is restricted to relatively short risk assessment time intervals near the conjunction's nominal TCA, because it uses 2-body propagation that neglects orbital perturbations that affect the motion over longer time scales. CDM mode can only be applied to single, temporally-isolated conjunctions with durations that are very short relative to the minimum orbital period of the two objects.
7. When comparing P_c estimates between BFMC's CDM and VCM modes, great care must be exercised to ensure that same model and environmental data sets, $\mathcal{D}$, have been used for both calculations. Specifically, to enable comparisons for a pre-existing CDM, a "check-out" procedure must be passed to ensure that the correct data files for $\mathcal{D}$ have been assembled.
8. No major statistical deviations have been detected between BFMC's CDM and VCM mode P_c estimates for 373 temporally-isolated conjunctions with 2D-$P_c > 1.5\times10^{-3}$ analyzed in this study, all of which were extracted from CARA's database of actual events and passed the required check-out procedure. This close alignment reflects the fact that the CDM mode samples equinoctial orbital states instead of Cartesian states.
9. A small fraction of temporally-isolated conjunctions show statistically significant deviations between BFMC's CDM mode P_c estimates and the 2D P_c approximation, based on analysis of 28,652 CARA archived conjunctions with 2D-$P_c > 10^{-7}$.
10. Many of the infrequent conjunctions found to have major BFMC-P_c vs 2D-P_c differences involve highly eccentric orbits, extended propagation times, or long separations between the TCA and the time of peak probability rate.
11. Close approach distance distributions provide insight into the infrequent conjunctions that have major BFMC-P_c vs 2D-P_c differences. Specifically, BFMC "conjunction b-plane" CA distributions can possess a curvature that is notably absent in 2D P_c distributions.

FUTURE WORK

The CARA team continues to study the optimal use of applying the BFMC VCM mode to extended or repeating conjunctions, such as those to occur between closely spaced objects or those in geosynchronous/geostationary orbit. Research also continues into the causes and characteristics of the observed BFMC-P_c vs 2D-P_c differences, with the goal of developing a robust and efficient set of tests that indicate the conditions for which the 2D P_c method provides an adequate approximation. Ideally, this study will be based on the examination of a very large (~1,000,000) number of conjunctions, and investigate conjunction parameters that have been used in the past (e.g., relative velocity, conjunction duration) as well as new possibilities (e.g., the difference between the TCA and the time of peak P_c rate, or the time of minimum Mahalanobis distance).

APPENDIX A: DEFINITION OF THE CONJUNCTION B-PLANE

For the k^{th} MC trial, the CA relative position and velocity of the primary and secondary can be used to define a "conjunction b-plane reference frame." The z-axis of this reference frame aligns with the CA relative velocity, given by the ECI unit vector

$$\hat{\mathbf{Z}}_{\boldsymbol{ca}}^{\boldsymbol{k}} = \frac{\mathbf{v}_2(t_{ca}^k) - \mathbf{v}_1(t_{ca}^k)}{|\mathbf{v}_2(t_{ca}^k) - \mathbf{v}_1(t_{ca}^k)|} \tag{12}$$

The (x,y) plane of this reference frame constitutes the b-plane itself. The (x,y) axes can be oriented in a variety of ways, but are defined here so that the b-plane's y-axis aligns as closely as possible to the ECI frame's z-axis, $\hat{\mathbf{z}}$, as follows

$$\hat{\mathbf{X}}_{\boldsymbol{ca}}^{\boldsymbol{k}} = \frac{\hat{\mathbf{Z}}_{\boldsymbol{ca}}^{\boldsymbol{k}} \times \hat{\mathbf{z}}}{|\hat{\mathbf{Z}}_{\boldsymbol{ca}}^{\boldsymbol{k}} \times \hat{\mathbf{z}}|} \qquad \text{and} \qquad \hat{\mathbf{Y}}_{\boldsymbol{ca}}^{\boldsymbol{k}} = \hat{\mathbf{Z}}_{\boldsymbol{ca}}^{\boldsymbol{k}} \times \hat{\mathbf{X}}_{\boldsymbol{ca}}^{\boldsymbol{k}} \tag{13}$$

Other (x,y) axis orientations could be defined by aligning to the local radial direction, or to the relative position vector of the mean states at the nominal TCA.

The CA relative position vector, $\mathbf{r}_2(t_{ca}^k) - \mathbf{r}_1(t_{ca}^k)$, can be transformed into the conjunction b-plane frame, yielding the following three Cartesian coordinates

$$X_{ca}^k = \hat{\mathbf{X}}_{\boldsymbol{ca}}^{\boldsymbol{k}} \cdot [\mathbf{r}_2(t_{ca}^k) - \mathbf{r}_1(t_{ca}^k)] \tag{14}$$

$$Y_{ca}^k = \hat{\mathbf{Y}}_{\boldsymbol{ca}}^{\boldsymbol{k}} \cdot [\mathbf{r}_2(t_{ca}^k) - \mathbf{r}_1(t_{ca}^k)] \tag{15}$$

$$Z_{ca}^k = 0 \tag{16}$$

MC CA distributions can be illustrated on X-Y scatter plots, as shown in Figure 5, by plotting a dot at the coordinates $\left(X_{ca}^k, Y_{ca}^k\right)$ for each sampling trial, $k = 1 \ldots N_s$. Figure 5 shows hits as red dots and misses as blue dots. The entire CA distribution on the b-plane can extend for very large distances (top panels), so an expanded or zoomed-in view (bottom panels) may be required to visualize better the hard-body protection radius, H, plotted as a green circle in Figure 5.

SYMBOLS AND ACRONYMS

a_f = the 2nd equinoctial orbital element
a_g = the 3rd equinoctial orbital element
B = Ballistic coefficient SP state parameter
$\boldsymbol{\mathcal{D}}$ = collected ensemble of model and environmental data sets required for SP propagation
H = the combined primary+secondary hard-body radii, or the hard-body protection distance
i = index for state vectors; $i = 1 \ldots 8$ for full SP states; $i = 1 \ldots 6$ for equinoctial element states
j = index for time bins, $j = 1 \ldots N_{bin}$
k = index for MC sampling trials, $k = 1 \ldots N_s$
n = The 1st equinoctial orbital element, the mean motion
$\mathcal{N}$ = a multi-variate normal (MVN) function
N_{bin} = the total number of time bins used to span a risk assessment interval $\tau_a < t \leq \tau_b$
$N_c(t_a, t_b)$ = the number of MC collisions or hits registered during the time interval $t_a < t \leq t_b$
N_s = the total number of MC sampling trials conducted in the simulation
$\mathbf{P}$ = SP state uncertainty covariance matrix
$\mathbf{P}_0$ = SP state uncertainty covariance matrix at the OD epoch time
$\mathbf{P}_{1,0}$ = SP covariance matrix at the OD epoch time for the primary object
$\mathbf{P}_{2,0}$ = SP covariance matrix at the OD epoch time for the secondary
$\mathbf{P}_1'$ = Equinoctial element TCA covariance matrix for the primary object

$\mathbf{P}_2'$ = Equinoctial element TCA covariance matrix for the secondary object
P_c = collision probability
$\tilde{P}_c(t_a, t_b)$ = P_c estimated from an MC simulation for the time interval $t_a < t \leq t_b$
S = Solar radiation pressure SP state parameter
$\mathbf{r}$ = ECI position vector
$\mathbf{r}_1$ = ECI position vector for the primary object
$\mathbf{r}_2$ = ECI position vector for the secondary
$\mathbf{r}_1'$ = ECI position vector for the primary propagated from TCA using 2-body equations of motion
$\mathbf{r}_2'$ = ECI position vector for the secondary propagated from TCA using 2-body equations of motion
$r_{2,1}^k$ = distance between the primary and secondary objects for the k^{th} sampling trial
$\dot{r}_{2,1}^k$ = time derivative of $r_{2,1}^k$
r_{ca}^k = CA distance between the primary and secondary objects for the k^{th} sampling trial
R_c = collision probability rate
$\tilde{R}_c$= R_c estimated from an MC simulation
$\mathcal{R}_{\text{CDM}}$ = BFMC CDM mode single-CPU computation rate [trials/CPUsec]
$\mathcal{R}_{\text{VCM}}$ = BFMC VCM mode single-CPU computation rate coefficient [(trials PROPday)/CPUsec]
T_j = midpoint time for the j^{th} time bin
t = time
t_0 = OD epoch time
$t_{1,0}$ = OD epoch time for the primary object
$t_{2,0}$ = OD epoch time for the secondary object
t_{ca}^k = CA time for the k^{th} sampling trial
t_{fc} = time of first contact
$\mathbf{v}_1$ = ECI velocity vector for the primary object
$\mathbf{v}_2$ = ECI velocity vector for the sedcondary object
$\mathbf{V}$ = matrix of eigenvectors
$\mathbf{V}_i$ = the eigenvector occupying the i^{th} column of $\mathbf{V}$
$\mathbf{x}$ = SP state deviation vector
$\mathbf{x}_0$ = SP state deviation vector at epoch
$\mathbf{X}$ = SP state vector
$\mathbf{X}_0$ = SP state vector at the OD epoch time
$\mathbf{X}_{0,\text{actual}}$ = the actual SP state vector at the OD epoch time, $\mathbf{X}_{0,\text{actual}} = \overline{\mathbf{X}}_0 + \mathbf{x}_0$
$\overline{\mathbf{X}}$ = mean SP state vector
$\overline{\mathbf{X}}_0$ = mean SP state vector at the OD epoch time
$\overline{\mathbf{X}}_{1,0}$ = mean SP state vector at the OD epoch time for the primary object
$\overline{\mathbf{X}}_{2,0}$ = mean SP state vector at the OD epoch time for the secondary object
$\overline{\mathbf{X}}'$ = mean equinoctial element TCA vector at a conjunction's nominal TCA
$\overline{\mathbf{X}}_1'$ = mean equinoctial element TCA vector for the primary object
$\overline{\mathbf{X}}_2'$ = mean equinoctial element TCA vector for the secondary object
$X_{ca}^k = X_{CA}^k$ = x-axis component of the CA distance in the conjunction b-plane for the k^{th} MC trial
$\hat{\mathbf{X}}_{ca}^k$ = ECI x-axis unit vector of the conjunction b-plane reference frame for the k^{th} MC trial
$\mathbf{Y}^k$ = the k^{th} sampled state
$\mathbf{Y}_{1,0}^k$ = the k^{th} sampled state at the OD epoch time for the primary object
$\mathbf{Y}_{s,0}^k$ = the k^{th} sampled state at the OD epoch time for the secondary object
$Y_{ca}^k = Y_{CA}^k$ = y-axis component of the CA distance in the conjunction b-plane for the k^{th} MC trial
$\hat{\mathbf{Y}}_{ca}^k$ = ECI y-axis unit vector of the conjunction b-plane reference frame for the k^{th} MC trial
$\hat{\mathbf{z}} = [0, 0, 1]^T$ = Cartesian z-axis unit vector

$\hat{\mathbf{Z}}_{ca}^{k}$ = ECI z-axis unit vector of the conjunction b-plane reference frame for the k^{th} MC trial

χ = The 4th equinoctial orbital element
$\delta T = \Delta T/2$ = time bin half width
ΔT = time bin width or duration
Δ(UT1-UTC) = difference between coordinated and universal time
λ_M = The 6th equinoctial orbital element, the mean longitude
$\mathbf{\Lambda}$ = diagonal matrix of eigenvalues
Λ_i = the eigenvalue occupying the i^{th} diagonal element of $\mathbf{\Lambda}$
ψ = The 5th equinoctial orbital element
ρ_0 = the epoch state uncertainty PDF
ϱ_i^k = a normally-distributed random deviate for the i^{th} component of the k^{th} sampled state
τ_a = beginning time of a risk assessment interval
τ_b = ending time of a risk assessment interval

ASW = Astrodynamics Support Workstation
BFMC = brute force Monte Carlo
CA = closest approach
CARA = Conjunction Assessment Risk Analysis
CDM = Conjunction Data Message
CPU = computational processing unit
CPUsec = one CPU second
DCA = Dynamic Calibration Atmosphere
ECI = Earth-Centered Inertial
HASDM = High Accuracy Satellite Drag Model
MC = Monte Carlo
MVN = multi-variate normal
NPD = non-positive definite
OD = orbit determination
PDF = probability density function
PROPday = one day of high fidelity SP propagation
SP = Special Perturbations
TCA = time of closest approach
UT1 = Universal Time corrected for polar motion
UTC = Coordinated Universal Time
VCM = Vector Covariance Message

ACKNOWLEDGMENTS

The authors would like to thank Russell Carpenter, Joseph Frisbee, Matthew Hejduk, Travis Lechtenberg, and Daniel Snow for several helpful discussions and analyses.

REFERENCES

[1] L.K. Newman and M.D. Hejduk, "NASA Conjunction Assessment Organizational Approach and the Associated Determination of Screening Volume Sizes," *International CA Risk Assessment Workshop*, 19-20 May 2015.
[2] B.D. Tapley, B.E. Schutz, and G.H. Born, *Statistical Orbit Determination*, Elsevier Academic Press, Burlington, MA, 2004.

[3] J.L. Foster and H.S. Estes, "A Parametric Analysis of Orbital Debris Collision Probability and Maneuver Rate for Space Vehicles," NASA/JSC-25898, Aug. 1992.
[4] K. Chan, *Spacecraft Collision Probability*, El Segundo, CA, The AeroSpace Corporation, 2008.
[5] S. Alfano, "Satellite Conjunction Monte Carlo Analysis," *AAS SpaceFlight Mechanics Meeting*, Pittsburgh, PA, Paper 09-233, Feb. 2009.
[6] D.A. Vallado, *Fundamentals of Astrodynamics and Applications*, 2rd ed., Microcosm Press, El Segundo CA, 2001.
[7] C. Sabol, C. Binz, A. Segerman, K. Roe, and P.W. Schumacher, Jr., "Probability of Collisions with Special Perturbations using the Monte Carlo Method," *AIAA/AAS Astrodynamics Specialist Conference*, Girdwood, AK, Paper 11-435, Aug. 2011.
[8] B.R. Bowman et. al., "A New Empirical Thermospheric Density Model JB2008 Using New Solar and Geomagnetic Indices," *AIAA/AAS Astrodynamics Specialist Conference*, Honolulu, HI, Paper AIAA 2008-6348, 2008.
[9] S.J. Casali and W.N. Barker, "Dynamic Calibration Atmosphere (DCA) for the High Accuracy Satellite Drag Model (HASDM)," *AIAA/AAS Astrodynamics Specialist Conference*, Monterey, CA, Paper AIAA 2002-4888, 2002.
[10] Air Force Space Command, "Astrodynamic Standards Software," http://www.afspc.af.mil, 2018.
[11] National Research Council of the National Academies, "Continuing Kepler's Quest Assessing Air Force Space Command's Astrodynamics Standards," *The National Academies Press*, 2012.
[12] M.R. Akella and K.T. Alfriend, "The Probability of Collision Between Space Objects," *Journal of Guidance, Control, and Dynamics*, Vol. 23, No. 5, pp. 769-772, 2000.
[13] V.T. Coppola, "Including Velocity Uncertainty in the Probability of Collision between Space Objects," *AAS/AIAA Spaceflight Mechanics Meeting*, Charleston SC, Paper 12-247, Feb. 2012.
[14] K.J. DeMars, Y. Cheng, and M.K. Jah, "Collision Probability with Gaussian Mixture Orbit Uncertainty," *Journal of Guidance, Control, and Dynamics*, Vol. 37, No. 3, pp. 979–985, 2014.
[15] B.A. Jones and A. Doostan, "Satellite Collision Probability Estimation Using Polynomial Chaos Expansions," *Advances in Space Research*, Vol. 52, pp. 1860-1875, 2013.
[16] K. Chan, "Formulation of Collision Probability with Time-Dependent Probability Distribution Functions," *AAS/AIAA Space Flight Mechanics Meeting*, Williamsburg, VA, Paper 15-233, Jan. 2015.
[17] K. Chan, "Hovering Collision Probability," *AAS/AIAA Space Flight Mechanics Meeting*, Williamsburg, VA, Paper 15-234, Jan. 2015.
[18] D.T. Hall, M.D. Hejduk, and L.C. Johnson, "Time Dependence of Collision Probabilities During Satellite Conjunctions," *AAS SpaceFlight Mechanics Meeting*, San Antonio, TX, Paper 17-271, 2017.
[19] J.L. Junkins, M.R. Akella, and K.T.Alfriend, "Non-Gaussian Error Propagation in Orbital Mechanics," *Journal of the Astronautical Sciences*, Vol. 44, No. 4, pp. 541-563, 1996.
[20] R.S. Park and D.J. Scheeres, "Nonlinear Mapping of Gaussian Statistics: Theory and Applications to Spacecraft Trajectory Design," *Journal of Guidance, Control, and Dynamics*, Vol. 29, No. 6, pp. 1367-1375, 2006.
[21] C. Sabol, T. Sukut, K. Hill, K. Alfriend, B. Write, Y. Li, and P. Schumacher, "Linearized Orbit Covariance Generation and Propagation Analysis via Simple Monte Carlo Simulations," *AAS/AIAA Space Flight Mechanics Meeting*, San Diego, CA, Paper 10-134, 2010.
[22] R.A. Broucke and P. J. Cefola, "On the Equinoctial Orbit Elements," *Celestial Mechanics*, Vol. 5, pp. 303-310, 1972.
[23] D. Vallado, "Covariance Transformation for Satellite Flight Dynamics Operations," *AAS/AIAA Astrodynamics Specialist Conference*, Big Sky, MT, Paper 03-526, 2003.
[24] D. Vallado and S. Alfano, "Updated Analytical Partials for Covariance Transformations and Optimization," *AAS/AIAA Space Flight Mechanics Meeting*, Williamsburg, VA, Paper 15-537, 2015.

[25] D.T. Hall, M.D. Hejduk, and L.C. Johnson, "Remediating Non-Positive Definite State Covariances for Collision Probability Estimation," *AAS Astrodynamics Specialist Conference*, Columbia Valley, WA, Paper 17-567, 2017.
[26] W.H. Press, S.A. Teukolsky, W.T. Vettering, and B.B. Flannery, *Numerical Recipes in FORTRAN: The Art of Scientific Computing*, 2nd Ed., Cambridge University Press, New York, NY, 1992.
[27] B.Schilling, *et al.* "Operational Experience with the Wald Sequential Probability Ratio Test for Conjunction Assessment from the Magnetospheric MultiScale Mission," *AAS Astrodynamics Specialist Conference*, Long Beach, CA, Paper 16-5424, 2016.
[28] C. Clopper and E.S. Peason, "The Use of Confidence or Fiducial Limits Illustrated in the Case of the Binomial," *Biometrika*, Vol. 26, pp 404-413, 1934.
[29] N.L. Johnson, S. Kotz, and A.W. Kemp, *Univariate Discrete Distributions*, Wiley-Interscience, Hoboken, NJ, 1993.
[30] L.D. Brown, T.T. Cai, A. Dasgupta, "Interval Estimation for a Binomial Proportion," *Statistical Science*, Vol. 16, No. 2, pp. 101-133, 2001.
[31] V.T. Coppola, "Evaluating the Short Encounter Assumption of the Probability of Collision Formula," *AAS/AIAA Spaceflight Mechanics Meeting*, Charleston SC, Paper 12-248, Feb. 2012.
[32] B.M. Braun, "The Evolution of Secondary Object Positions in 18SCS Conjunction Data Messages," *AAS Astrodynamics Specialist Conference*, Columbia Valley, WA, Paper 17-650, 2017.
[33] V.T. Coppola, J. Woodburn, and R. Hujsak, "Effects of Cross Correlated Covariance on Spacecraft Collision Probability," *AAS/AIAA Spaceflight Mechanics Meeting*, Wailea Maui, HI, Paper 04-181, Feb. 2004.
[34] S. Casali, D. Hall, D. Snow, M. Hejduk, L. Johnson, B. Skrehart, and L. Baars, "Effect of Cross-Correlation of Orbital Error on Probability of Collision Determination," *AAS Astrodynamics Specialist Conference*, Snowbird, UT, Paper 18-272, Aug. 2018.
[35] *NIST/SEMATECH* "Engineering Statistics Handbook," *E-Handbook of Statistical Methods*, Section 7.3.3, https://www.itl.nist.gov/div898/handbook/prc/section3/prc33.htm, 2018. Also see https://www.itl.nist.gov/div898/software/dataplot/refman1/auxillar/binotest.htm, 2018.
[36] A. Sergeyevsky, G. Snyder, R. Cuniff, *Interplanetary Mission Design Handbook, Volume 1, Part 2. Earth to Mars Ballistic Mission Opportunities, 1990-2005*, NASA JPL Publication 82-43, 1983.